Environmental Science and Pollution Research (2020) 27:14044–14057
https://doi.org/10.1007/s11356-020-07756-x

RESEARCH ARTICLE

The role of bentonite clay and bentonite clay@MnFe2O4 composite and their physico-chemical properties on the removal of Cr(III) and Cr(VI) from aqueous media

Amir Ahmadi[1] · Rauf Foroutan[2] · Hossein Esmaeili[1] · Sajad Tamjidi[3]

Received: 24 November 2019 / Accepted: 14 January 2020 / Published online: 8 February 2020

Abstract

In this investigation, bentonite clay (BC) and bentonite clay@MnFe2O4 composite (BCMFC) were applied as efficient adsorbents for adsorbing Cr(III) and Cr(VI) ions from aqueous media. Different analyses such as FTIR, SEM, EDX, Map, BET, and XRD were used to characterize the adsorbents. The results showed that the removal efficiency of Cr(III) and Cr(VI) using BC were found to be 95.21 and 95.74%, while the corresponding values to the BCMFC were 97.37 and 98.65%, respectively. Also, the equilibrium and kinetic studies showed that the Freundlich isotherm model and the quasi-second-order kinetic model could better describe the equilibrium and kinetic behaviors of the adsorption process. The maximum adsorption capacity of the BC for the adsorption of Cr(III) and Cr(VI) ions were evaluated as 151.5 mg/g (25oC, pH 6, 90 min, and 1 g/L) and 161.3 mg/g (25oC, pH 3, 90 min, and 1 g/L), respectively, while the BCMFC showed the maximum capacities of 175.4 mg/g (25oC, pH 6, 60 min, and 1.5 g/L) and 178.6 mg/g (25oC, pH 3, 60 min, and 1.5 g/L) for Cr(III) and Cr(VI) ions, respectively, which were remarkable amounts. In addition, the thermodynamic study indicated that the adsorption process was physical, spontaneous, and exothermic. High removal efficiency, high chromium adsorption capacity, and low-cost magnetic adsorbent were significant features of the BCMFC for removal of Cr (III) and Cr (VI).

Keywords Clay · Clay@MnFe2O4 composite · Cr (III) ion · Cr (VI) ion · Adsorption

Introduction

During the past decades, the rapid development of various industries has led to an increase in the contamination of aqueous environments with heavy metal ions and raising serious problems around the world. Heavy metal contamination represents a major environmental concern due to the toxicity, non-biodegradability, carcinogenicity, and environment-stability of the heavy metals, which make them accumulate within the body of living creatures and enter the so-called food chain to have it contaminated (Pawar et al. 2016). As a heavy metal, the chromium and its derivatives are being used in a wide range of industries including chemical plants, leather production industries, steel plants, dye and pigment production, coal combustions, plating of metals, and the textile industry, finding their ways into the environment through the wastewater produced at such industries (Samuel et al. 2018). In an aqueous environment, this metal exhibits two oxidation species, namely chromium (III) and chromium (VI). Compared with Cr(III), Cr(VI) exhibits higher levels of toxicity (500–1000 times as large as the Cr(III)) and carcinogenicity together with superior solubility and mobility in aqueous media (Xie et al. 2019; Tamjidi and Esmaeili 2019). It should be noted that in contrast to Cr(VI), Cr(III) has lower toxicity and represents a necessary requirement for glucose metabolism in the human body (Tamjidi and Esmaeili 2019; Maleki et al. 2015). Once introduced into the body of living organisms, Cr(VI) can lead to different disorders such as allergy, itching, and irritation of the skin, nasal irritations and bleeding, ulceration, genetic mutations, liver and kidney damages,

Responsible editor: Tito Roberto Cadaval Jr

✉ Hossein Esmaeili
esmaeili.hossein@iaubushehr.ac.ir; esmaeili.hossein@gmail.com

[1] Department of Chemical Engineering, Bushehr Branch, Islamic Azad University, Bushehr, Iran

[2] Faculty of Chemical and Petroleum Engineering, University of Tabriz, Tabriz 5166616471, Iran

[3] Department of Chemical Engineering, Shiraz Branch, Islamic Azad University, Shiraz, Iran

attenuated immune system, and even fatality (Dinari and Haghighi 2018). Considering the adverse impacts of the Cr(VI) ion on the living organisms and the environment, WHO and EPA have reported the allowable content of this metal ion in drinkable and surface waters as 0.05 and 0.1 mg/L, respectively (Dima et al. 2015). This highlights the necessity of treating the chromium ion-contaminated wastewater from different industries before disposing the wastewater into the environment.

Among the conventional methods for the removal of heavy metal ions from aqueous media, there are different physical-chemical methods such as ion exchange, chemical deposition, membrane processes, extraction, filtration, oxidation, reverse osmosis, electrochemical, and adsorption method (Foroutan et al. 2019a, b). Today, thanks to its widespread of advantages including low-cost, easy operation, high selectivity, and availability of various adsorbents, the adsorption method has been widely regarded by researchers (Abbasi et al. 2019). This method has been acknowledged as a conventional yet environment-friendly method as it can be implemented using renewable biomasses and natural compounds as adsorbent (Tamjidi et al. 2019). During the recent past, various natural compounds have been examined as adsorbent for the adsorption and removal of heavy metal ions from aqueous solutions; examples of such adsorbents include sawdust of eucalyptus, date palm, and sour lemon (Esmaeili and Foroutan 2019), Fe3O4 nanoparticles (Yue et al. 2016), bone char–ZnO composite (Ranjbar et al. 2018), *Sargassum oligocystum* (Yeganeh et al. 2019), eggshell (Elabbas et al. 2016), *Populus alba* activated carbon (Bonyadi et al. 2019), pillared clays (Mnasri-Ghnimi and Frini-Srasra 2019), graphene oxide (Pang et al. 2019; Liu et al. 2019), and smectites (D'Ascanio et al. 2019). Thanks to its large active surface area and high adsorption capacity for adsorbing heavy metals from aqueous media, activated carbon is often used for this purpose. In the meantime, this material is still used for removing the metals and other water contaminants on a large scale because of its significant disadvantages including limited reducibility and high synthesis cost (Bhatnagar and Minocha 2010). The clay has recently attracted great deals of attention as an adsorbent due to its abundant in the environment, low production cost, large surface area, and high mechanical and chemical resistance (Foroutan et al. 2019c; Karapinar and Donat 2009). The use of chemically modified clay as an adsorbent has been frequently studied in several previous works (Kurniawan et al. 2011). In the present study, MnFe2O4 particles were used to enhance the properties and increase the adsorption capacity of the bentonite clay (BC) by increasing the interaction between active sites of an adsorbent and the contaminant.

The present research is aimed at investigating the adsorption capability of the BC and bentonite clay@MnFe2O4 composite (BCMFC) for removing the Cr(III) and Cr(VI) metal ions from aqueous media. The adsorbents were further characterized using different analyses (FTIR, SEM, EDX, Map, XRD, and BET). Also, to determine the exothermic/endothermic and chemical/physical nature of the adsorption process, the thermodynamic and equilibrium studies were done.

Experimental section

Materials

The BC studied in this research was prepared from the mines around Dashtestan city, Bushehr Province, Iran. Sodium hydroxide (NaOH, Sigma Aldrich Company, purity ≥ 0.97), iron chloride hexahydrate (FeCl3.6H2O, Sigma Aldrich Company, purity≥0.98), hydrochloric acid (HCl 37%, Merck Company), manganese chloride tetrahydrate (MnCl2.4H2O, Sigma Aldrich Company, purity ≥ 0.99), potassium di-chromate (K2Cr2O7, Sigma Aldrich Company, purity ≥ 0.99), and chromium(III) nitrate nonahydrate (Cr(NO3)3.9H2O, Sigma Aldrich Company, purity ≥ 0.99.99) were procured and used as received. The stock solutions (1000 mg/L) containing the Cr(III) and Cr(VI) ions were prepared by dissolving predetermined amounts of potassium dichromate and chromium (III) nitrate nonahydrate in distilled water. To provide solutions with lower concentrations of Cr (III) and Cr (VI), the stock solutions were diluted using distilled water. It is worth mentioning that all of the chemicals used in this study were used without further purification.

Preparing the adsorbents

The BC sorbent was collected from mines at Bushehr Province (Iran) and it was then dried in an oven at 105 °C for 24 h to achieve full dehydration. The dried clay was then powdered in a mill and graded through the sieve no. 25 (ASTM E11) followed by storage in anti-moisture bottles at ambient temperature. To prepare the BCMFC adsorbent, an aqueous solution containing manganese (II) and iron (III) in a molar ratio of 2:1 was prepared. Next, 1 g of the prepared BC was added to the solution followed by mixing on a magnetic stirrer for 40 min to have Fe+3 and Mg+2 ions located on the BC surface layers. Subsequently, the solution temperature was raised to 60–70 °C before adding sodium hydroxide solution (5 mol/L) to adjust the pH value to 11; the resultant solution was then stirred for 1 h. The prepared composite was then removed from the solution and washed several times with distilled water to completely neutralize. The neutralized composite was heated in the oven at 105 °C for 24 h to become fully dehydrated and ready for being used as an adsorbent (Podder and Majumder 2015). Figure 1 shows the aforementioned procedure to produce adsorbent and its use for the removal of Cr (III) and Cr (VI) ions from aqueous media.

Fig. 1 A procedure for production of adsorbent and its use to remove Cr (III) and Cr (VI) from aqueous media

Batch adsorption test

The adsorption process of Cr(III) and Cr(VI) ions using powder of BC and clay@MnFe2O4 was done using the following procedure. Firstly, to check the effect of pH value on the sorption efficiency, 100 mL of aqueous solution containing Cr(III) or Cr(VI) was introduced into a 250 mL Erlenmeyer flask, followed by adjusting the pH value in the range of 2–8. Next, adsorption tests were performed under a particular set of conditions (temperature = 25 °C, Ci = 10 mg/L, contact time = 60 min, adsorbent dosage = 1 g/L, and mixing rate = 400 rpm). Following each test, the solid phase (adsorbent) was eliminated from the liquid phase (aqueous media) and concentration of the considered metal ion in the aqueous phase was evaluated using a flame atomic absorption spectrophotometer. Once finished with determining the optimal value of pH, effects of other parameters, including the contact time (5–120 min), initial metal ion concentration (10–300 mg/L), temperature (25–50 °C) and adsorbent dosage (0.25–4 g/L) on the adsorption efficiency were studied at the optimum pH value. In each stage, after performing the adsorption test, the used adsorbents were eliminated from the synthetic wastewater and 20 mL of the solution stored for further analysis to specify the chromium ion content by the flame atomic absorption spectrophotometer (Analytik Jena novAA® 400). Adsorption efficiency (R) and chromium ion adsorption capacity (qe) per each gram of sorbent (mg/g) were obtained from Eqs. (1) and (2):

$$R\% = \frac{C_i - C_e}{C_i} \times 100 \quad (1)$$

$$q_e = \frac{C_i - C_e}{w} \times V \quad (2)$$

where Ci and Ce (mg/L) are the primary and equilibrium doses of the chromium ion, respectively, V is the aqueous media volume (L), and W is the weight of the adsorbent (g). In all cases, the adsorption tests were performed in triplicates and average values were reported.

Apparatus and equipment

The FTIR analysis (Bruker Victor 22 spectrometer) was used to determine the functional groups existing in the BC and the BCMFC, and also assess the interactions between the functional groups and chromium ions after the adsorption process. The FTIR analyses were done within the wavenumber range of 400–4000 cm^{-1}. Moreover, using a Siemens D500

diffractometer, X-ray diffraction (XRD) analysis was conducted in 2θ angles between 5 and 80° and wavelength of 1.5048 Å to determine the crystalline phases in the adsorbent. Scanning electron microscopy (SEM, FEG-TESCAN MIRA3) was used to study surface changes and determining the distribution of different elements in the BC and BCMFC. Moreover, Brunauer-Emmett-Teller (BET, Micrometrics ASAP 2020, USA) was used to measure surface properties including the porosity and the specific surface area of the adsorbents. Furthermore, Vibrating Sample Magnetometer (VSM, Lakeshore 7400, USA) analysis was used to determine the adsorbent magnetic characteristics in the range of − 8000 to 8000 Oe.

Results and discussion

Characterizations of the adsorbents

The FTIR analyses from the BC and the BCMFC adsorbents before and after the adsorption process are displayed in Fig. 2a. The figure shows the spectra both prior to and after the adsorption. The results showed adsorption peaks on the spectra recorded from the prepared BC and the BCMFC in the ranges of 3431–3843 cm^{-1} and 1632–1645 cm^{-1}, respectively, which might be attributed to stretching vibrations of the O-H functional groups (Al-OH or deformation of the water molecules) in the structure of the adsorbents (Mobarak et al. 2018). Moreover, low-intensity vibrations were observed in the range of 2854–2868 cm^{-1} and at 2979 cm^{-1} in the structure of the BC and the BCMFC, which corresponded to the vibrations of the C-H functional group in the mentioned structures (Acisli et al. 2016). In the BC structure, several peaks were seen in the range of 519–790 cm^{-1}; this could be linked to asymmetric stretching vibrations of the Si-O-Mg, Si-O-Al, and Si-O-Si and also bending vibrations of the Si-O in the structure of the BC and the BCMFC (Bertagnolli et al. 2011). Both adsorbents exhibited a sharp peak in the range of 1026–1029 cm^{-1}, which corresponded to the stretching vibrations of the silica (Si-O) in the structure of the used adsorbents (Thue et al. 2018). Upon the formation of the BCMFC, changes were evident in the ranges and intensities of the peaks as compared with the BC. These changes could be resulted from the interactions between the functional groups in the structure of the BCMFC and the placement of the MnFe2O4 nanoparticles in the BC structure. Following the sorption process of Cr(III) and Cr(VI) ions on the considered adsorbents, the range and intensity of the vibrations related to the functional groups on the adsorbents changed abruptly, as is clear by comparing the respective spectra. The significant changes in the range and intensity of the peaks could be a result of the interactions between functional groups on the adsorbents and Cr(III) and Cr(VI) ions. Therefore, the results of the FTIR analysis indicated that the MnFe2O4 nanoparticles were successfully embedded into the BC structure and that the used adsorbents were well capable of adsorbing Cr(III) and Cr(VI) ions from aqueous solutions.

Figure 2b shows the XRD spectra for the clay, MnFe2O4 nanoparticles, and the BCMFC. According to this figure, the BC exhibited various peaks at different intensities, including quartzite (SiO2), diaspore (AlOOH), muscovite, and hematite (Fe2O3) (Selmani et al. 2017). On the XRD spectrum recorded from the BC, several peaks were observed at 2θ values of 23.22, 25.64, 31.23, 37.27, 47.65, 50.24, 61.42, and 64.72°, indicating the presence of quartzite, montmorillonite, muscovite, muscovite, quartzite, calcite, and montmorillonite,

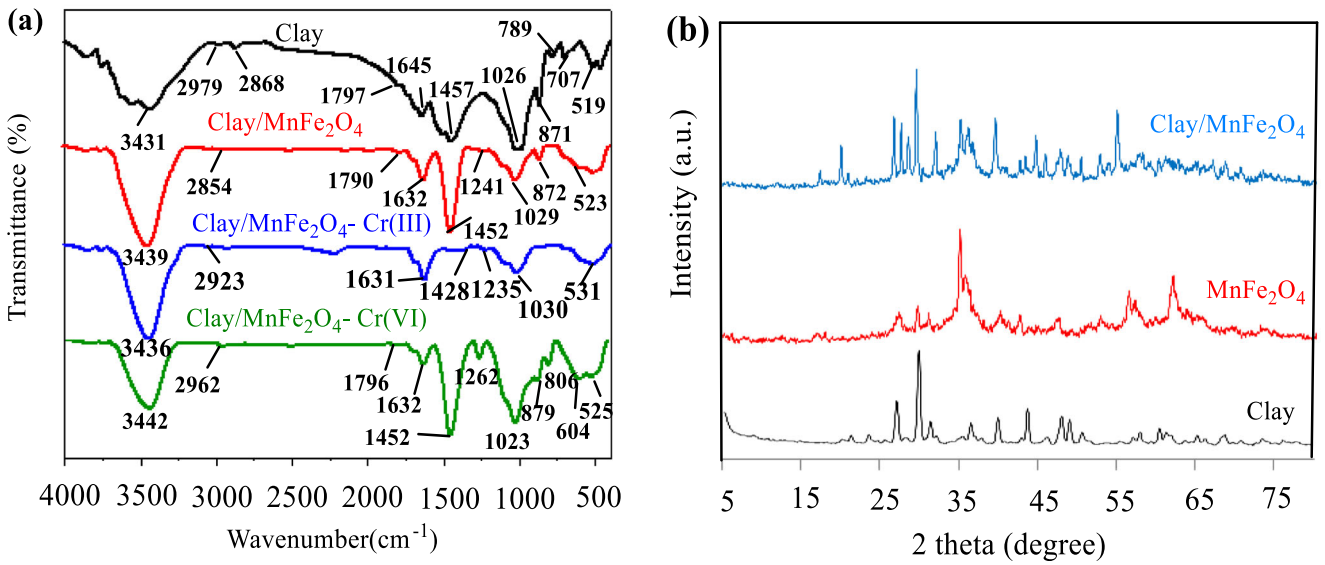

Fig. 2 FTIR analyses on the BC and BCMFC before and after the sorption process (**a**) and XRD analyses on the BC, MnFe2O4 nanoparticles, and BCMFC (**b**)

respectively. On the XRD spectrum recorded from the MnFe2O4 nanoparticles, several peaks were also observed at 2θ values of 18.04, 29.6, 35.02, 42.2, 52.62, 56.24, and 61.74°, indicating the presence of the following crystalline phases in the magnetized nanoparticles of MnFe2O4, respectively: (111), (220), (311), (400), (422), (333), and (440) (Ghobadi et al. 2018). Upon the formation of the BCMFC, the peaks characterizing the MnFe2O4 nanoparticles were observed on the spectrum recorded from the prepared composite, indicating good interaction between the BC and the magnetic nanoparticles, i.e. the MnFe2O4 nanoparticles were successfully embedded into the BC structure.

In order to investigate the morphology and particle surface variations of the sorbents, EDX, Map and SEM analyses were performed both before and after the adsorption of ions, with the results shown in Fig. 3. The results showed the presence of a variety of pores with a wide range of pore size on the surface of the BC; the pore space could contribute to not only the adsorption process but also the placement of the MnFe2O4 nanoparticles on the layers of the clay (Fig. 3a). The results of the EDX and Map analyses indicated the presence of different elements on the surface of the BC, including aluminum, magnesium, silicon, calcium, and iron, with the elements distributed uniformly across the BC surface (Fig. 3b, c). After the formation of the BCMFC, particles of various sizes with an almost spherical morphology were placed on the surface of the BC; these could be a result of the formation of the MnFe2O4 nanoparticles on the surface and within the layers of the BC (Fig. 3d). Notably, the results of the EDX and Map analyses affirmed the successful formation of the MnFe2O4 nanoparticles on the surface of the BC. Upon the formation of the composite, the content of iron and manganese ions in the composite increased, confirming the successful synthesis of the BCMFC (Fig. 3e, f). After applying the BCMFC as an adsorbent for the adsorption of the chromium ion, significant changes were observed in the composite surface, and the chromium ions were observed in the structure of the adsorbent, highlighting the capability of the magnetized composite for adsorbing the chromium ion. In addition, the results of EDX analyses showed that the magnetized composite could better adsorb the Cr(VI) ion rather than the Cr(III) ion (Fig. 3i, l), which is in accord with the experimental results and the maximum adsorption capacity.

Figure 4 displays the adsorption-desorption isotherm for the BC, MnFe2O4 and the BCMFC. It was investigated to study such characteristics as average pore size, specific surface area, and pore volume. Based on the results of BET analysis, pore size, specific surface area, and pore volume for the BC were reported as 102.32 Å, 15.64 m2/g, and 0.04 cm3/g, respectively. Also, pore size, specific surface area, and pore volume for the BC were reported as 74.49 Å, 196.56 m2/g, and 0.366 cm3/g, respectively. In addition, the BET results revealed that the mentioned quantities for the BCMFC were equal to 121.29 Å, 95.92 m2/g, and 0.29 cm3/g, respectively. It is worth mentioning that, according to IUPAC, both of the studied samples exhibited mesoporous structures with increased specific surface area by more than 6% once the MnFe2O4 particles were placed on the surface of the BC. The increase in the specific surface area of the BCMFC, as compared with the BC, can enhance the adsorption capacity of the adsorbent.

Finally, Fig. 5. shows the VSM analysis for the MnFe2O4 and BCMFC adsorbents. According to the results, the saturation magnesium for the MnFe2O4 and BCMFC adsorbents were obtained 31.88 and 13.28 emu/g, respectively. The reason for this difference can be attributed to the size of particles and concentration of oxygen adsorbed on the particles (Foroutan et al. 2018b, 2019d). Also, the results show that both magnetic materials have ferromagnetic properties (Xia et al. 2016). In addition, it is noteworthy that the difference between hysteresis loops for aforementioned samples is small and their behavior is close to paramagnetic.

Effect of pH value

The pH value is among the most key factors contributing to the sorption process as it affects the availability of active sites on the adsorbent surface and the existing ions in the aqueous media. To check the impact of pH on the efficiency of the chromium ion adsorption using the BCMFC, studies were performed at different pH values in the range of 3–8 (Fig. 6). The obtained results showed that with increasing the pH, the adsorption efficiency of the Cr(VI) ion decreased using both adsorbents. The maximum adsorption efficiency of the Cr(VI) ion using the BC (92.75%) and the BCMFC (98.65%) obtained at an initial pH value of 3. At higher pH values, the Cr(VI) ion adsorption efficiency decreased using both adsorbents; this decrease could be attributed to different factors. At higher pH values, metal ions (including the Cr(VI) ion) precipitate in the form of hydroxides and reduce the ion concentration in the solution, which results in a decrease in the adsorption efficiency (Geetha et al. 2016). Moreover, the drop in the Cr(VI) ion adsorption yield by increasing the pH value can be attributed to the resultant change in the surface charge of the adsorbents (from positively charged to negatively charge) that generates some repulsive electrostatic force between ions and the sorbent surface (Du et al. 2015). By increasing the pH value in the range of 2–6, the Cr(III) ion adsorption efficiency using the BC and the BCMFC increased from 28.65 and 48.53% to 92.23 and 97.37%, respectively. Further increase in the pH value beyond 6, decreased the Cr(III) ion adsorption efficiency using both sorbents. So, the pH value of 6 was reported as the optimal pH value for the Cr(III) ion adsorption process. The lower adsorption efficiencies of Cr(III) ion at sub-6 pH values could be due to the presence of hydronium ion (H+) in the aqueous medium. In this case, H+ ions

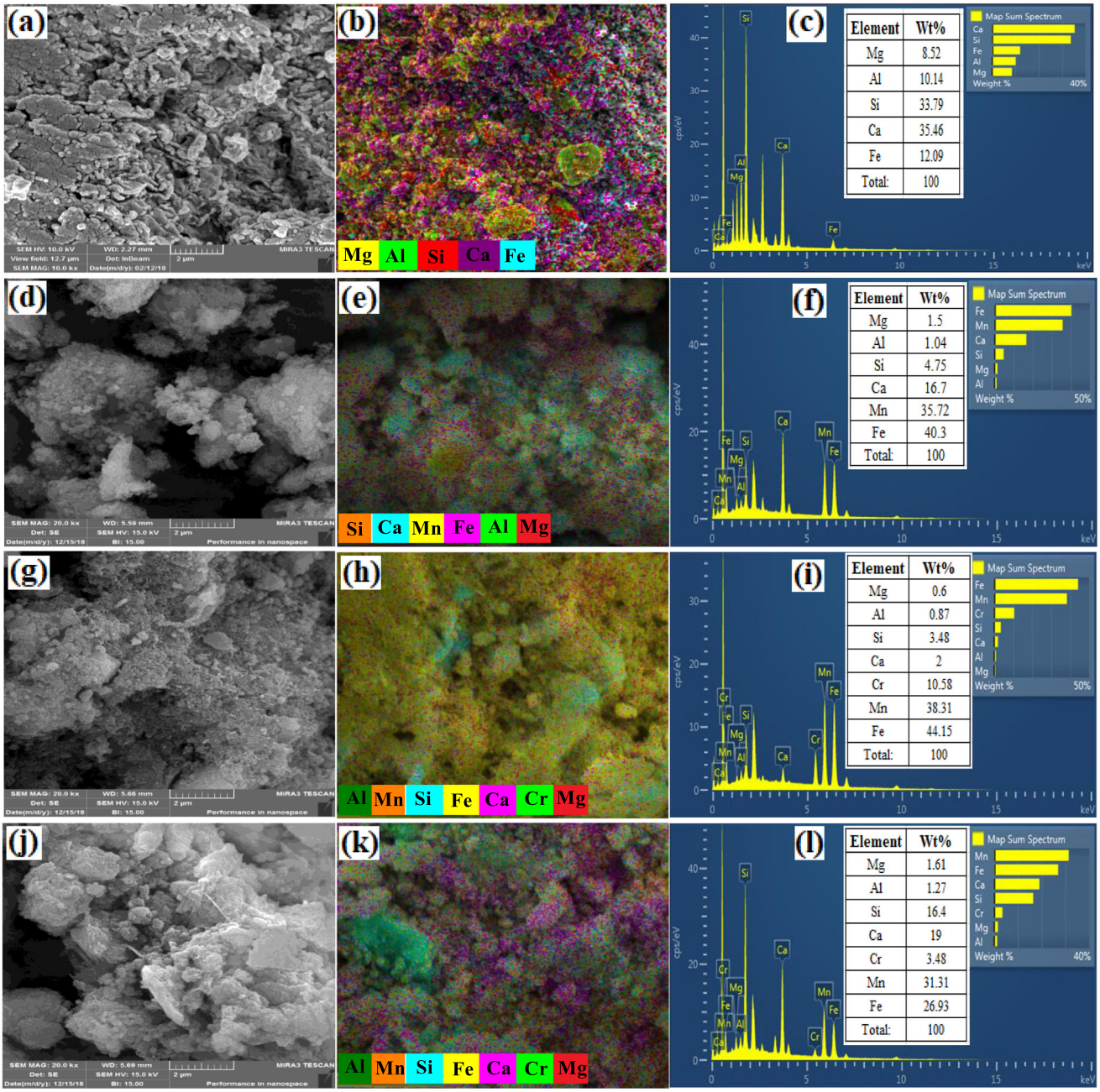

Fig. 3 EDX, map, and SEM analyses on the BC (**a**–**c**), BCMFC (**d**–**f**), BCMFC after sorption of Cr(VI) ion (**g**–**i**), and BCMFC after sorption of Cr(III) ion (**j**–**l**)

compete with Cr(III) ion for occupying the active sites on the adsorbent while protonating the nitrogen on the surface of the adsorbents, thereby attenuating the interactions between the Cr(III) ion and the adsorbent surface (Dinari and Haghighi 2018). The reduction in the Cr(III) and Cr(VI) adsorption efficiency on the studied adsorbents at pH values below 2 could be attributed to the acidic decomposition of the MnFe2O4 nanoparticles and dissolution of the organic components of the adsorbents at such pH values (Jin et al. 2018). Finally, the initial pH values of 3 and 6 were identified as optimal pH values for the sorption of Cr(VI) and Cr(III) ions, respectively.

Effects of time and sorbent dosage

Figure 7a demonstrates the impact of contact time on the sorption efficiency of Cr(VI) and Cr(III) ions using the considered sorbents. The results demonstrate that the chromium ion sorption using these adsorbents is carried out in two steps, with the first stage showing higher rate and adsorption efficiency. The

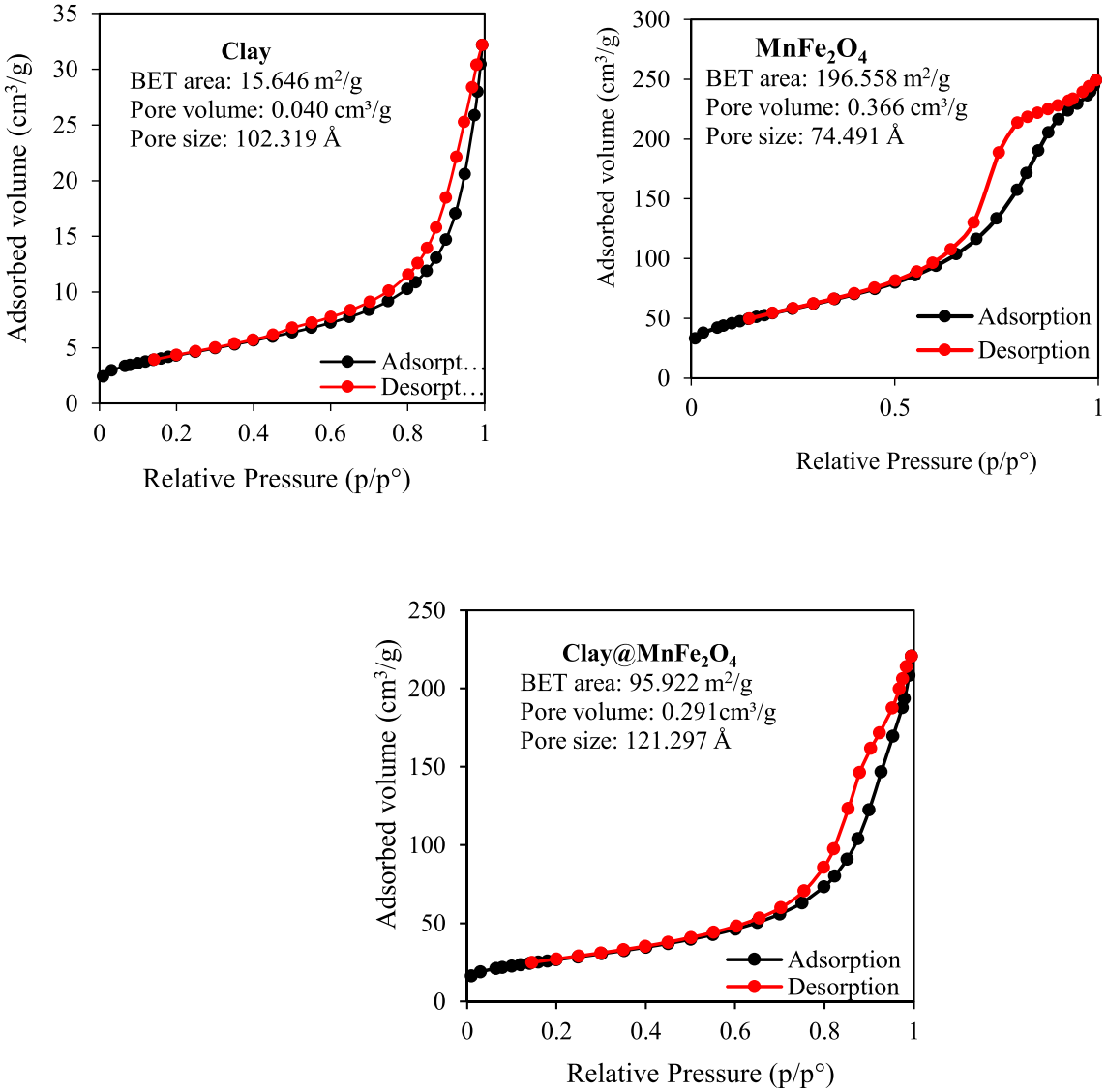

Fig. 4 Adsorption-desorption isotherm of nitrogen on the BC, MnFe2O4, and BCMFC

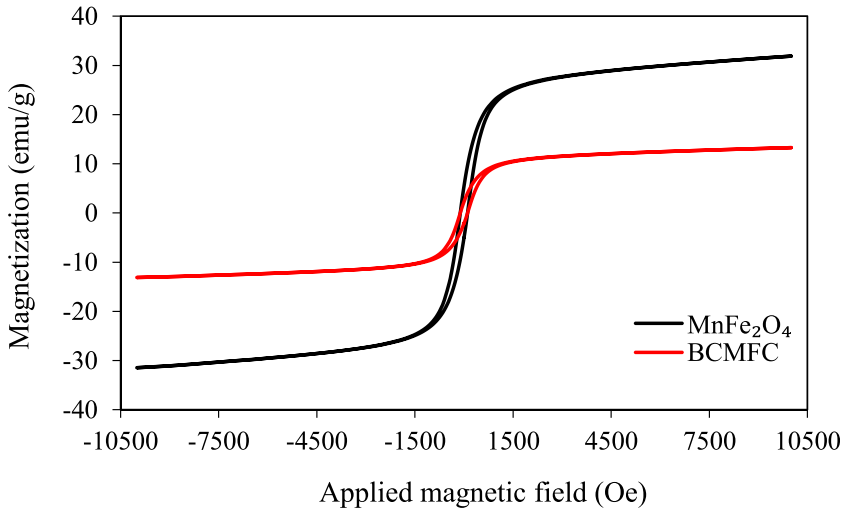

Fig. 5 VSM analyses for MnFe2O4 and BCMFC

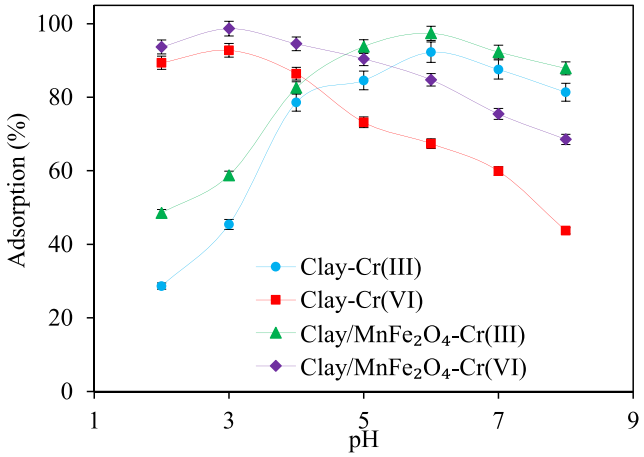

Fig. 6 Effect of pH on the adsorption efficiency of Cr(III) and Cr(VI) ions from aqueous media using the BC and BCMFC (temperature: 25 °C, initial ion concentration: 10 mg/L, contact time: 60 min, adsorbent dosage: 1 g/L, stirring rate: 400 rpm)

first stage of the adsorption process took 5–60 min to occur and was based on the availability of vacant active sites and

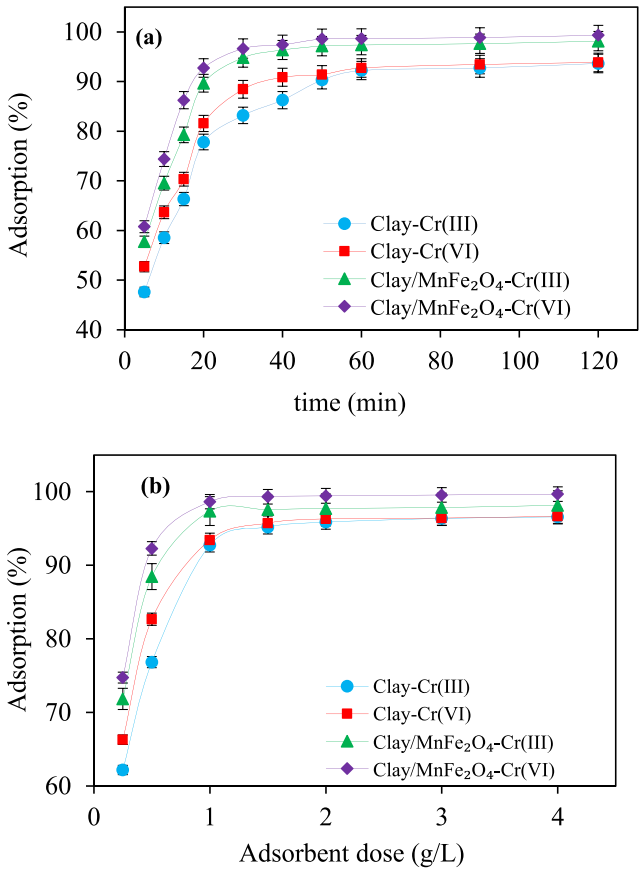

Fig. 7 **a** Effect of contact time on the adsorption efficiency of Cr(III) and Cr(VI) ions from aqueous media (temperature: 25 °C, initial ion concentration: 10 mg/L, adsorbent dosage: 1 g/L, stirring rate: 400 rpm); **b** effect of the sorbent dose on the adsorption efficiency (at optimal pH value, contact time for the BC as adsorbent: 90 min, contact time for the BCMFC as adsorbent: 60 min, initial ion concentration: 10 mg/L, temperature: 25 °C, stirring rate: 400 rpm)

appropriate surface condition for placing the chromium ions on the sorbent surface (Foroutan et al. 2019a). The rate of chromium ion adsorption on the surface of the adsorbents was significantly decreased at contact times beyond 60 min, possibly because of the saturation of the available active sites on the sorbent surface of the or inaccessibility of the existing active sites on the adsorbent surface for the chromium ions. Accordingly, the equilibrium contact time for the sorption of Cr(VI) and Cr(III) ions using both adsorbents was reported as 60 min.

The sorbent dosage is another key factor imposing large contributions to the sorption process, as it can determine the adsorption efficiency of the sorbent for a given initial concentration of the contaminant (heavy metals) (Habiby et al. 2019). In this respect, the impact of the sorbent dosage on the adsorption efficiency of Cr(III) ad Cr(VI) ions was investigated in the range of 0.25–4 g/L, and the outcomes are indicated in Fig. 7b. According to the outcomes, the chromium ion adsorption yield enhanced abruptly by increasing the adsorbent dosage from 0.25 g/L to up to 1.5 g/L, beyond which no considerable changes were seen in the chromium ion adsorption efficiency using the studied adsorbents. Based on the results, the optimal adsorbent dosages on the BC and the BCMFC were reported as 1 and 1.5 g/L, respectively.

Impact of temperature and thermodynamic study

Impact of temperature on the adsorption of Cr(III) and Cr(VI) ions using the studied adsorbents was examined in the temperature range of 25–50 °C (Fig. 8a). By increasing the temperature from 25 °C to 50 °C, Cr3+ and Cr6+ ions adsorption efficiencies decreased, showing the exothermic nature of the sorption process using the studied adsorbents. The reduction in the adsorption efficiency using the studied adsorbents could also be a result of shrinkage and hence changed surface area of active sites on the adsorbents (Abshirini et al. 2019a).

In the present study, in order to determine the adsorption behavior of the Cr(III) and Cr(VI) ions on the BC and the BCMFC, three thermodynamic parameters were investigated in the temperature range of 25–50 °C. These parameters included the standard enthalpy variation (ΔH°), the standard entropy variation (ΔS°), and the standard Gibbs free energy variation (ΔG°). The other parameters affecting the adsorption process were set to the optimal values obtained in the previous stages. The thermodynamic parameters were evaluated using eqs. 3 and 4 (Foroutan et al. 2019b):

$$\Delta G^o = -RTln(1000K_D) \tag{3}$$

$$ln(1000K_D) = \frac{-\Delta H^o}{RT} + \frac{\Delta S^o}{R} \tag{4}$$

where *R*, *T*, and *KD* are defined as the universal gas constant

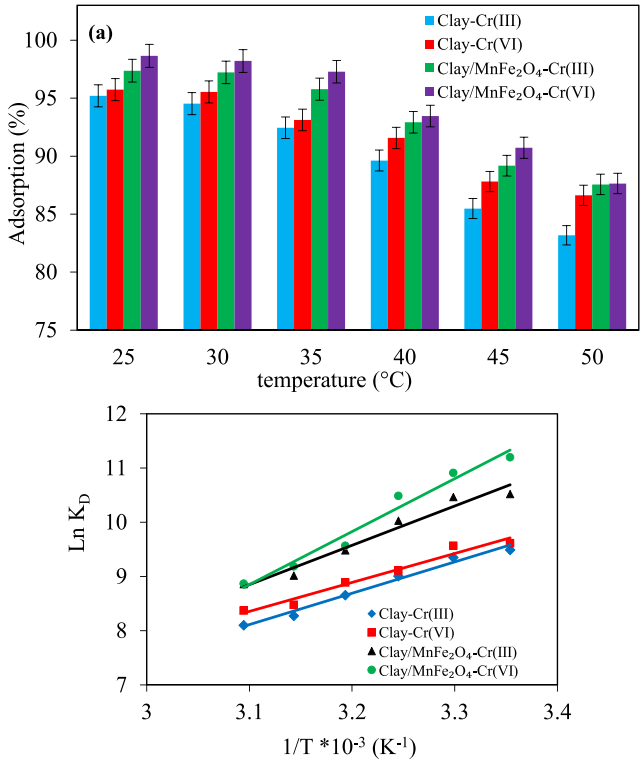

Fig. 8 Effect of temperature on the adsorption efficiency of Cr(III) and Cr(VI) ions from aqueous media using the BC and BCMFC (at optimal pH value, contact time of 90 min for the BC and 60 min for the BCMFC, initial ion concentration: 10 mg/L, optimal adsorbent dosage, stirring rate: 400 rpm) (**a**), and the linear relationship between ln *KD* and 1/*T* (**b**)

(8.314 J/mol.K), temperature (K), and the equilibrium constant (1000 $\frac{q_e}{C_e}$), respectively. In addition, the terms ΔH° and ΔS° are evaluated as the slope and intercept obtained from Fig. 8. The results are reported in Table 1. Negative ΔG° values were reported for the Cr(III) and Cr(VI) ions adsorption process using the adsorbents in the temperature range of 25–50 °C. The negative value of this parameter represents that the adsorption process is favorable and spontaneous (Kundu and Mondal 2019). The obtained value of the ΔH° for the adsorption process was also negative, leading us to the conclusion that the interactions between the adsorbent surface and the Cr(III) and Cr(VI) heavy metals were exothermic in nature. Based on the results, the ΔS° value for the Cr(III) and Cr(VI) sorption was negative, indicating a reduction in the random collision of the chromium ion and the sorbent surface in the sorption process (Esmaeili and Foroutan 2019).

Kinetic study

To check the kinetic behavior of the Cr(III) and Cr(VI) ions sorption process from the aqueous media using the BC and BCMFC adsorbents, quasi-first-order (eqs. 5) and quasi-second-order (eqs. 6) kinetic models, as well as intraparticle diffusion model (eqs. 7) were used and the linear form of these models are presented as follows:

$$\ln\left(q_{eq}-q_t\right) = \ln q_{eq.cal} - K_1 t \tag{5}$$

$$\frac{t}{q_t} = \frac{1}{K_2 q_{eq}^2} + \frac{t}{q_{e.cal}} \tag{6}$$

$$q_t = K_I t^{0.5} + I \tag{7}$$

where *qeq* and *qt* in terms of mg/g are the adsorbed amount of the chromium ion per gram of the adsorbent at equilibrium time, respectively. Also, *K*1 and *K*2 are the adsorption constants for the quasi-first-order (1/min) and quasi-second-order kinetic models (g/mg.min) and *KI* is also the intraparticle diffusion adsorption constant (mg/g.min0.5). The constants and kinetic parameters of the sorption process were specified using the linear relationships describing the respective models (Fig. 9), with the outputs tabulated in Table 2. The kinetics of the sorption process of the chromium ions on the aforesaid sorbents were performed using the experimental data. The impact of contact time on the chromium ion sorption efficiency using the aforementioned adsorbents was evaluated under a particular set of test conditions, including 25 °C, chromium concentration of 10 mg/L, sorbent dosage of 1 g/L, 400 rpm stirring rate, and optimal pH.

Based on the obtained results, the deviation of the sorption capacities obtained via the quasi-first-order kinetic model from the respective laboratory data was much larger than that of the quasi-second-order kinetic model. This indicates a lower capability of the pseudo-first-order kinetic model for investigating the kinetic behavior of the sorption process, as compared with the pseudo-second-order kinetic model. In addition, the obtained values for the correlation coefficient (*R*2) in the quasi-second-order kinetic model for the adsorption of Cr(III) and Cr(VI) ions were greater than of that for the quasi-first-order kinetic model, further confirming the higher capability of the quasi-second-order kinetic model for describing the kinetic behavior of the sorption process. Moreover, the intraparticle diffusion model was described that the chromium ion adsorption process was nonlinear, indicating that more than one type of process contributes to ions sorption on the considered sorbents (Hameed 2009). The initial linear part of the figure has a higher slope and is related to the film diffusion in which metal ions are transported to the adsorbent. This stage was done at a high rate. The second linear section has a lower slope, which shows metal ion diffusion into the aforesaid adsorbent (Yürüm et al. 2014).

Equilibrium study

In the present study, in order to check the equilibrium behavior of the chromium ions sorption from the aqueous media using

Table 1 The thermodynamic parameters considered to study the Cr(III) and Cr(VI) ions adsorption process using the BC and the BCMFC

Adsorbent	T(oC)	ΔG°(KJ/moL)	ΔH°(KJ/moL)	ΔS° (J/moL.K)
Clay-Cr (III)	25	− 23.528	− 48.178	− 81.926
	30	− 23.570		
	35	− 23.076		
	40	− 22.541		
	45	− 21.888		
	50	− 21.764		
Clay/MnFe2O4-Cr(III)	25	− 26.075	− 60.330	− 113.469
	30	− 26.378		
	35	− 25.696		
	40	− 24.687		
	45	− 23.848		
	50	− 23.801		
Clay-Cr (VI)	25	− 23.833	− 44.433	− 68.282
	30	− 23.653		
	35	− 23.333		
	40	− 23.139		
	45	− 22.422		
	50	− 22.147		
Clay/MnFe2O4-Cr(VI)	25	− 27.761	− 81.266	− 178.352
	30	− 27.504		
	35	− 26.871		
	40	− 24.908		
	45	− 24.302		
	50	− 23.821		

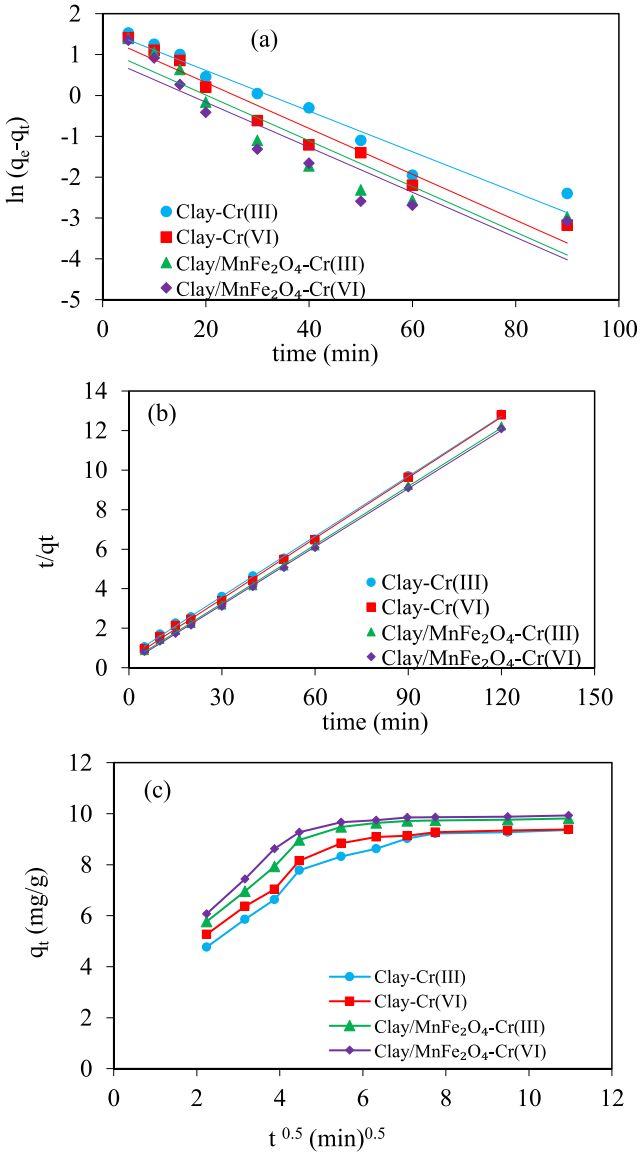

Fig. 9 Linear relationships expressing the quasi-first-order and second-order kinetic models as well as the intraparticle diffusion model for the adsorption of Cr(III) and Cr(VI) ions from aqueous media

the BC and BCMFC, the Freundlich, Langmuir, and Dubinin–Radushkevich (D–R) models were utilized with the definitions expressed in eqs. 8–10, respectively.

$$\frac{C_e}{q_e} = \frac{1}{k_L \times q_m} + \frac{C_e}{q_e} \tag{8}$$

$$lnq_e = lnk_F + \frac{1}{n} \times lnC_e \tag{9}$$

$$lnq_e = lnq_m - \beta\varepsilon^2 \tag{10}$$

where *qe* is the equilibrium adsorption capacity (mg/g), *Ce* is the equilibrium concentration of chromium ion in the aqueous solution (mg/L), *qm* is the maximum sorption capacity (mg/g), *KL* is the sorption energy (L/g), *KF* and *n* are the constants of the Freundlich model, β is the activity coefficient indicating the free energy of adsorption (mol2/J2), and ε is the Polanyi potential $\left(\varepsilon = RT\ln\left(1 + \frac{1}{C_e}\right)\right)$. The linear relationships corresponding to the Freundlich, Langmuir, and R-D models are shown in Fig. 10a–c and the corresponding parameters to them are reported in Table 3. In order to investigate the equilibrium behavior of the sorption process, the equilibrium data corresponding the initial chromium ion concentrations was employed. The experimental conditions to investigate the equilibrium isotherms for each adsorbent and each ion were different. To do this, the equilibrium study for the removal of Cr (III) using the BC was studied at conditions: T = 25 oC, pH 6, contact time of 90 min, and the adsorbent dosage of 1 g/L. Also, these conditions for Cr(VI) removal by the BC was included: T = 25 oC, pH 3, contact time of 90 min, and the adsorbent dosage of 1 g/L. In addition, for the removal of Cr(III) using the BCMFC, the experiments were done at 25 oC, pH 6, contact time of 60 min, and the adsorbent dosage of 1.5 g/L. Moreover, these conditions for the removal of Cr(VI) using the BCMFC was included:

Table 2 Constants and kinetic parameters determined for the Cr(III) and Cr(VI) ions adsorption process

Kinetic model	Adsorbent			
	BC-Cr (III)	BC-Cr(VI)	BCMFC-Cr(III)	BCMFC-Cr(VI)
Pseudo-first order				
qe cal	4.99	4.214	3.085	2.547
K1	0.0498	0.0561	0.056	0.055
R2	0.955	0.9616	0.873	0.862
Pseudo-second order				
qe.cal	9.891	9.794	10.15	10.19
K2	0.017	0.024	0.031	0.039
R2	0.999	0.999	0.999	0.999
qe.exp	9.365	9.386	9.814	9.933
Intraparticle diffusion				
Ki,1 (mg/g min1/2)	1.313	1.246	1.413	1.459
I1 (mg/g)	1.748	2.428	2.549	2.841
R2	0.985	0.983	0.995	0.995
Ki,2 (mg/g min1/2)	0.445	0.187	0.148	0.120
I2 (mg/g)	5.856	7.849	8.682	8.997
R2	0.987	0.901	0.978	0.977
Ki,3 (mg/g min1/2)	0.044	0.035	0.024	0.021
I3 (mg/g)	8.876	9.008	9.548	9.698
R2	0.956	0.992	0.946	0.939

25oC, pH 3, contact time of 60 min, and the adsorbent dosage of 1.5 g/L.

By applying the Langmuir model, the correlation coefficients for the sorption of Cr(III) and Cr(VI) ions were in the range of 0.9122–0.9436 (Table 3), which was generally lower than those obtained for the Freundlich model; this indicates that the equilibrium data followed the Freundlich isotherm model. The maximum sorption capacities of Cr3+ and Cr6+ on the BC were obtained as 151.51 and 161.29 mg/g, respectively. The adsorption capacities using the BCMFC adsorbent were also achieved as 175.44 and 178.57 mg/g, respectively. Such high values indicated an enhancement in the sorption amount upon modifying the BC with the MnFe2O4 nanoparticles. This enhancement could be attributed to the increased active surface of the BCMFC compared with the BC, as was evident from the results of the BET analyses. As a characteristic of the Langmuir isotherm model, the dimensionless parameter RL $\left(R_L = \frac{1}{1+k_L C_o}\right)$ specifies the type of sorption process and the corresponding isotherm. Accordingly, if $RL > 1$, $RL = 1$, $RL = 0$, and $0 < RL < 1$, the adsorption process is characterized as undesirable, linear, irreversible, and desirable, respectively (Foroutan et al. 2018a). The value of the parameter RL for the Cr3+ and Cr6+ ions adsorption on the considered adsorbents fell within the range of 0–1, indicating the desirability of the chromium ion sorption process using these sorbents. In addition, the value of n for this adsorption process was evaluated to exceed 1, showing that the physical and favorable nature of the adsorption process. Besides RL and n, average free energy (E) represents another important parameter that evaluates the sorption process in terms of its physical or chemical nature; this parameter can be computed using the D-R model. If the value of the average free energy of the adsorption is within the range of 8–16 kJ/mol, the adsorption process will characterize as going through an ion-exchange mechanism, while average free energies is lower than 8 kJ/mol shows that the sorption process is based on a physical mechanism. Based on the results obtained in the present research, the value of the parameter E for the sorption process was lower than 8 kJ/mol for the adsorbents, leading us to the conclusion that the sorption process is founded on a physical basis. According to the results obtained from the equilibrium study, one can draw that the chromium ion adsorption on the studied adsorbents is a favorable physical process where the equilibrium data follow the Freundlich isotherm model.

Furthermore, the maximum sorption capacity obtained in this research was compared with previous studies and the results are presented in Table 4. By comparing the results, it was found that the BC and BCMFC had considerable adsorption capacities in comparison with other adsorbents in the removal of Cr(III) and Cr(VI) ions from aqueous media.

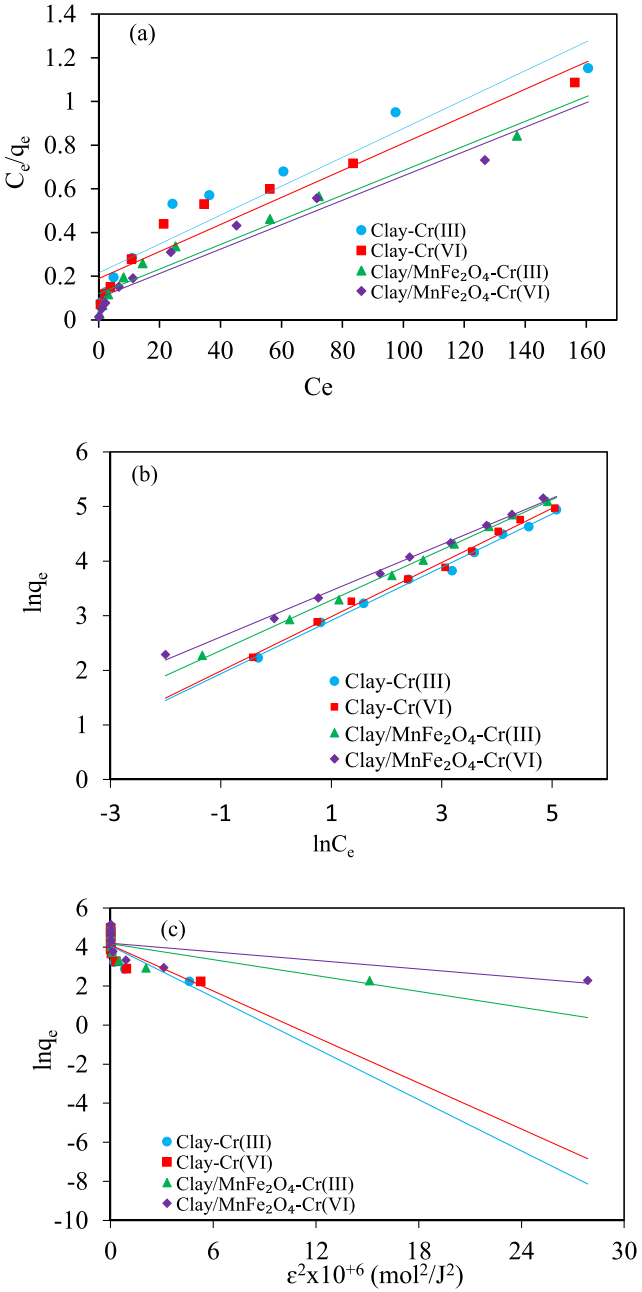

Fig. 10 Langmuir (**a**), Freundlich (**b**), and D-R (**c**) isotherm models for the adsorption of Cr(III) and Cr(VI) from aqueous media using the BC and BCMFC

Table 3 Constants and equilibrium study for the adsorption of the Cr(III) and Cr(VI) on the BC and the BCMFC

Models	Adsorbent/Ions			
	BC-Cr (III)	BCMFC-Cr(III)	BC-Cr (VI)	BCMFC-Cr(VI)
Langmuir				
qm (mg/g)	151.51	175.44	161.29	178.57
KL (L/mg)	0.031	0.046	0.033	0.053
RL	0.097–0.763	0.067–0.685	0.091–0.752	0.059–0.653
R2	0.912	0.944	0.925	0.930
Freundlich				
n	2.051	2.171	2.015	2.364
Kf (mg/g (L/mg)1/n)	11.307	16.854	12.016	20.796
R2	0.993	0.998	0.994	0.996
D-R				
E (KJ/mol)	1.068	1.918	1.128	2.608
qm (mg/g)	57.92	64.89	60.78	66.37
βx10–6(mol2/J2)	0.4379	0.1359	0.393	0.0735
R2	0.562	0.521	0.562	0.511

Conclusion

As a naturally occurring material, the BC has been widely applied and largely regarded thanks to its outstanding structure and properties. In the present research, the BC and the BCMFC were applied as efficient sorbents to recover and attenuate Cr(III) and Cr(VI) ions from aqueous media. The adsorption of chromium ions from aqueous solution on the considered adsorbents was performed discretely to evaluate the effect of different parameters on the sorption efficiency. The results showed that, compared with other parameters, the initial pH value imposed a larger impact on the adsorption efficiency, and an increase in the initial concentration of the Cr(III) and Cr(VI) decreased the adsorption efficiency. The Freundlich, Langmuir, and D-R isotherm models were used to study the equilibrium behavior of chromium ion adsorption process. The results showed that the adsorption process was favorable and physical in nature. Moreover, the Freundlich isotherm model outperformed the other isotherm models as per its higher value of correlation coefficient (*R*2). This sheds light on the fact that, compared with other models, the Freundlich model could better describe the equilibrium behavior of the adsorption process, with the heterogeneous surfaces, rather than homogeneous faces, imposing a larger impact on the adsorption process. The study on the kinetics of the adsorption process proved that the kinetic data corresponding to the Cr(III) and Cr(VI) adsorption processes follow a pseudo-second-order kinetic model regardless of the adsorbent used. In addition, results of the intraparticle diffusion model showed that the relationship proposed by the intraparticle diffusion model for the adsorption process was nonlinear. This shows that more than one process is involved with the ions sorption process, and that the sorption process could be influenced by the film-through and intraparticle diffusion mechanisms. The thermodynamic study was also showed that the adsorption process was physical ad exothermic. Therefore, due to the removal efficiencies obtained and the operating conditions, it is recommended to use the adsorbents formulated in this research to effectively remove chromium ion from aqueous solutions.

Table 4 Comparing the results with previous studies

Adsorbent	Maximum adsorption capacity of Cr (III) (mg/g)	Maximum adsorption capacity of Cr (VI) (mg/g)	Reference
Activated carbon	–	36.496	(Foroutan et al. 2018b)
Activated carbon/CoFe2O4	–	70.422	(Foroutan et al. 2018b)
Sargassum oligocystum algae biomass	–	34.46	(Foroutan et al. 2018c)
CaO/Fe3O4/SDS nanocomposite	6.406	–	(Tamjidi and Esmaeili 2019)
activated carbon prepared from Ziziphus spina-christi leaf	–	13.81	(Abshirini et al. 2019a)
magnetic core-shell Fe3O4@MoS2	–	324.3	(Yang et al. 2019)
MoS2@Fe3O4	–	290.2	(Yang et al. 2019)
MgO/Fe3O4 nanocomposite	–	23.9	(Abshirini et al. 2019b)
Bentonite clay	151.5	161.3	Present study
Bentonite clay/MnFe2O4	175.4	178.6	Present study

References

Abbasi S, Foroutan R, Esmaeili H, Esmaeilzadeh F (2019) Preparation of activated carbon from worn tires for removal of cu (II), Ni (II) and Co (II) ions from synthetic wastewater. Desalin Water Treat 141: 269–278

Abshirini Y, Foroutan R, Esmaeili H (2019a) Cr (VI) removal from aqueous solution using activated carbon prepared from Ziziphus spina-christi leaf. Mater Res Express 6(4):045607

Abshirini Y, Esmaeili H, Foroutan R (2019b) Enhancement removal of Cr (VI) ion using magnetically modified MgO nanoparticles. Mater Res Express 6(12):125513

Acisli O, Khataee A, Karaca S, Sheydaei M (2016) Modification of nanosized natural montmorillonite for ultrasound-enhanced adsorption of Acid Red 17. Ultrason Sonochem 31:116–121

Bertagnolli C, Kleinübing SJ, Da Silva MGC (2011) Preparation and characterization of a Brazilian bentonite clay for removal of copper in porous beds. Appl Clay Sci 53:73–79

Bhatnagar A, Minocha A (2010) Biosorption optimization of nickel removal from water using Punica granatum peel waste. Colloid Surface B 76:544–548

Bonyadi Z, Kumar PS, Foroutan R, Kafaei R, Arfaeinia H, Farjadfard S, Ramavandi B (2019) Ultrasonic-assisted synthesis of Populus alba activated carbon for water defluorination: application for real wastewater. Korean J Chem Eng 36(10):1595–1603

D'Ascanio V, Greco D, Menicagli E, Santovito E, Catucci L, Logrieco AF, Avantaggiato G (2019) The role of geological origin of smectites and of their physico-chemical properties on aflatoxin adsorption. Appl Clay Sci 181:105209

Dima JB, Sequeiros C, Zaritzky NE (2015) Hexavalent chromium removal in contaminated water using reticulated chitosan micro/nanoparticles from seafood processing wastes. Chemosphere 141: 100–111

Dinari M, Haghighi A (2018) Ultrasound-assisted synthesis of nanocomposites based on aromatic polyamide and modified ZnO nanoparticle for removal of toxic Cr (VI) from water. Ultrason Sonochem 41: 75–84

Du Y, Wang L, Wang J, Zheng G, Wu J, Dai H (2015) Flower-, wire-, and sheet-like MnO 2-deposited diatomites: highly efficient absorbents for the removal of Cr (VI). J Environ Sci 29:71–81

Elabbas S, Mandi L, Berrekhis F, Pons MN, Leclerc JP, Ouazzani N (2016) Removal of Cr (III) from chrome tanning wastewater by adsorption using two natural carbonaceous materials: eggshell and powdered marble. J Environ Manag 166:589–595

Esmaeili H, Foroutan R (2019) Adsorptive behavior of methylene blue onto sawdust of sour lemon, date palm, and eucalyptus as agricultural wastes. J Dispers Sci Technol 40:990–999

Foroutan R, Ahmadlouydarab M, Ramavandi B, Mohammadi R (2018a) Studying the physicochemical characteristics and metals adsorptive behavior of CMC-g-HAp/Fe3O4 nanobiocomposite. J Environ Chem Eng 6:6049–6058

Foroutan R, Mohammadi R, Ramavandi B, Bastanian M (2018b) Removal characteristics of chromium by activated carbon/CoFe 2 O 4 magnetic composite and Phoenix dactylifera stone carbon. Korean J Chem Eng 35(11):2207–2219

Foroutan R, Mohammadi R, Ramavandi B (2018c) Treatment of chromium-laden aqueous solution using CaCl 2-modified Sargassum oligocystum biomass: characteristics, equilibrium, kinetic, and thermodynamic studies. Korean J Chem Eng 35(1):234–245

Foroutan R, Oujifard A, Papari F, Esmaeili H (2019a) Calcined Umbonium vestiarium snail shell as an efficient adsorbent for treatment of wastewater containing Co (II). 3 biotech 9(3):78

Foroutan R, Mohammadi R, Farjadfard S, Esmaeili H, Saberi M, Sahebi S, Dobaradaran S, Ramavandi B (2019b) Characteristics and performance of cd, Ni, and Pb bio-adsorption using Callinectes sapidus biomass: real wastewater treatment. Environ Sci Pollut Res 26: 6336–6347

Foroutan R, Mohammadi R, Adeleye AS, Farjadfard S, Esvandi Z, Arfaeinia H, Sorial GA, Ramavandi B, Sahebi S (2019c) Efficient arsenic (V) removal from contaminated water using natural clay and clay composite adsorbents. Environ Sci Pollut Res 26:29748–29762

Foroutan R, Mohammadi R, Razeghi J, Ramavandi B (2019d) Performance of algal activated carbon/Fe3O4 magnetic composite for cationic dyes removal from aqueous solutions. Algal Res 40: 101509

Geetha P, Latha M, Pillai SS, Deepa B, Kumar KS, Koshy M (2016) Green synthesis and characterization of alginate nanoparticles and its role as a biosorbent for Cr (VI) ions. J Mol Struct 1105:54–60

Ghobadi M, Gharabaghi M, Abdollahi H, Boroumand Z, Moradian M (2018) MnFe2O4-graphene oxide magnetic nanoparticles as a high-performance adsorbent for rare earth elements: synthesis, isotherms, kinetics, thermodynamics and desorption. J Hazard Mater 351:308–316

Habiby SR, Esmaeili H, Foroutan R (2019) Magnetically modified MgO nanoparticles as an efficient adsorbent for phosphate ions removal from wastewater. Sep Sci Technol:1–12

Hameed B (2009) Evaluation of papaya seeds as a novel non-conventional low-cost adsorbent for removal of methylene blue. J Hazard Mater 162(2):939–944

Jin X, Liu Y, Tan J, Owens G, Chen Z (2018) Removal of Cr (VI) from aqueous solutions via reduction and absorption by green synthesized iron nanoparticles. J Clean Prod 176:929–936

Karapinar N, Donat R (2009) Adsorption behaviour of Cu2+ and Cd2+ onto natural bentonite. Desalination 249:123–129

Kundu A, Mondal A (2019) Kinetics, isotherm, and thermodynamic studies of methylene blue selective adsorption and photocatalysis of malachite green from aqueous solution using layered Na-intercalated Cu-doped Titania. Appl Clay Sci 183:105323

Kurniawan A, Sutiono H, Ju YH, Soetaredjo FE, Ayucitra A, Yudha A, Ismadji S (2011) Utilization of rarasaponin natural surfactant for organo-bentonite preparation: application for methylene blue removal from aqueous effluent. Micropor Mesopor Mat 142:184–193

Liu X, Ma R, Wang X, Ma Y, Yang Y, Zhuang L, Zhang S, Jehan R, Chen J, Wang X (2019) Graphene oxide-based materials for efficient removal of heavy metal ions from aqueous solution: a review. Environ Pollut 252:62–73

Maleki A, Hayati B, Naghizadeh M, Joo SW (2015) Adsorption of hexavalent chromium by metal organic frameworks from aqueous solution. J Ind Eng Chem 28:211–216

Mnasri-Ghnimi S, Frini-Srasra N (2019) Removal of heavy metals from aqueous solutions by adsorption using single and mixed pillared clays. Appl Clay Sci 179:105151

Mobarak M, Selim AQ, Mohamed EA, Seliem MK (2018) Modification of organic matter-rich clay by a solution of cationic surfactant/H 2 O 2: a new product for fluoride adsorption from solutions. J Clean Prod 192:712–721

Pang H, Wu Y, Wang X, Hu B, Wang X (2019) Recent advances in composites of Graphene and layered double hydroxides for water remediation: a review. Chem Asian J 14(15):2542–2552

Pawar RR, Bajaj HC, Lee SM (2016) Activated bentonite as a low-cost adsorbent for the removal of cu (II) and Pb (II) from aqueous solutions: batch and column studies. J Ind Eng Chem 34:213–223

Podder M, Majumder C (2015) Bacteria immobilization on neem leaves/MnFe2O4 composite surface for removal of as (III) and as (V) from wastewater. Arab J Chem

Ranjbar N, Hashemi S, Ramavandi B, Ravanipour M (2018) Chromium (VI) removal by bone char–ZnO composite: parameters optimization by response surface methodology and modeling. Environ Prog Sustain 37(5):1684–1695

Samuel SM, Subramaniyan V, Bhattacharya J, Chidambaram R, Qureshi T, Singh NP (2018) Ultrasonic-assisted synthesis of Graphene oxide–fungal hyphae: an efficient and reclaimable adsorbent for chromium (VI) removal from aqueous solution. Ultrason Sonochem

Selmani S, Sdiri A, Bouaziz S, Joussein E, Rossignol S (2017) Effects of metakaolin addition on geopolymer prepared from natural kaolinitic clay. Appl Clay Sci 146:457–467

Tamjidi S, Esmaeili H (2019) Chemically modified CaO/Fe3O4 nanocomposite by sodium dodecyl sulfate for Cr (III) removal from water. Chem Eng Technol 42:607–616

Tamjidi S, Esmaeili H, Moghadas BK (2019) Application of magnetic adsorbents for removal of heavy metals from wastewater: a review study. Mater Res Express 6:102004

Thue PS, Sophia AC, Lima EC, Wamba AG, de Alencar WS, dos Reis GS, Rodembusch FS, Dias SL (2018) Synthesis and characterization of a novel organic-inorganic hybrid clay adsorbent for the removal of acid red 1 and acid green 25 from aqueous solutions. J Clean Prod 171:30–44

Xia S, Xu X, Xu C, Wang H, Zhang X, Liu G (2016) Preparation, characterization, and phosphate removal and recovery of magnetic MnFe2O4 nano-particles as adsorbents. Environ Technol 37:795–804

Xie Y, Lin J, Liang J, Li M, Fu Y, Wang H, Tu S, Li J (2019) Hypercrosslinked mesoporous poly (ionic liquid) s with high density of ion pairs: efficient adsorbents for Cr (VI) removal via ion-exchange. Chem Eng J 378:122107

Yang S, Li Q, Chen L, Chen Z, Pu Z, Wang H, Yu S, Hu B, Chen J, Wang X (2019) Ultrahigh sorption and reduction of Cr (VI) by two novel core-shell composites combined with Fe3O4 and MoS2. J Hazard Mater 19:120797

Yeganeh G, Ramavandi B, Esmaeili H, Tamjidi S (2019) Dataset of the aqueous solution and petrochemical wastewater treatment containing ammonia using low cost and efficient bio-adsorbents. Data Brief 26:104308

Yue X, Guo W, Li X, Zhou H, Wang R (2016) Core-shell Fe 3 O 4@ MIL-101 (Fe) composites as heterogeneous catalysts of persulfate activation for the removal of Acid Orange 7. Environ Sci Pollut Res 23(15):15218–15226

Yürüm A, Kocabaş-Ataklı ZÖ, Sezen M, Semiat R, Yürüm Y (2014) Fast deposition of porous iron oxide on activated carbon by microwave heating and arsenic (V) removal from water. Chem Eng J 242:321–332